Non-Hermitian Cavity Quantum Electrodynamics - Configuration Interaction Singles Approach for Polaritonic Structure with *ab initio* Molecular Hamiltonians

Jonathan McTague[1] and Jonathan J. Foley IV[1]
William Paterson University, Department of Chemistry, 300 Pompton Road, Wayne NJ 07470, USA

(*Electronic mail: foleyj10@wpunj.edu)

(Dated: 20 October 2021)

We combine *ab initio* molecular electronic Hamiltonians with a cavity quantum electrodynamics model for dissipative photonic modes and apply mean-field theories to the ground- and excited-states of resulting polaritonic systems. In particular, we develop a restricted Hartree-Fock theory for the mean-field ground-state and a non-Hermitian configuration interaction singles theory for mean-field ground- and excited-states of the molecular system strongly interacting with a photonic mode, and apply these methods to elucidating the phenomenology of paradigmatic polaritonic systems. We leverage the Psi4Numpy framework to yield open-source and accessible reference implementations of these methods.

I. INTRODUCTION

The interaction between molecular excitations and nanoconfined photons can produce the requisite strong interactions for polaritonic chemistry[1–29]. Motivated by a desire to provide a realistic picture of the molecular structure under the influence of strong photonic interaction, there has been a recent surge in activity focused on merging *ab initio* molecular electronic structure theory with cavity quantum electrodynamics (*ab initio* CQED) to provide an accurate and predictive model of polaritonic chemistry[9,24,27,30–35]. Such efforts include combining CQED with density functional theory (DFT) or it's time-dependent extension (TDDFT)[30,35–39], reduced density matrix mechanics[34], and wavefunction theory using the coupled-cluster ansatz[24,27,33]. Such approaches can provide access to potential energy surfaces, couplings, and other properties of interest for simulating the structure and reactivity of polaritonoic chemical systems.

The role of photonic dissipation or cavity losses on polaritonic structure and dynamics has recently been discussed in a number of studies utilizing model Hamiltonians[18,23,25,29], though to our knowledge the effort to pursue *ab initio* CQED methods has not explicitly included photonic loss. In this context, photonic dissipation refers to the finite lifetime of occupied photonic modes that exist within a cavity. Photonic dissipation occurs because the photons confined within a cavity can couple to the material degrees of freedom that exist in the cavity itself (which can be significant when considering plasmonic cavities), and also to the continuum of modes that exist outside the cavity (which causes leakage of photons in Fabry-Perot cavities, for example)[18,25,40]. In this work we present a simple *ab initio* CQED method for treating ground and excited polaritonic states with explicit inclusion of photonic lifetimes via a non-Hermitian cavity quantum electrodynamics - configuration interaction singles approach (NH-CQED-CIS). This approach provides a simplification for the couplings between photon and material degrees of freedom that contribute to photon dissipation, and subsumes these complicated interactions into a complex frequency of the photon that quantifies the sum of all photon dissipation rates[25,40]. Setting the imaginary part of the frequency in this approach implies a lossless photonic mode that is perfectly isolated from the environment and returns the formulation to a Hermitian CQED-CIS theory. We implement this approach in the coherent state basis which results from solution of the CQED-Hartree-Fock (CQED-HF) equations. We endeavor to provide a detailed picture of the key equations and algorithmic considerations for both the CQED-HF and NH-CQED-CIS approach, and also provide reference implementations through the Psi4Numpy project[41]. We apply both methods to the analysis of several paradigmatic systems, including the ground-state polaritonic structure of formaldehyde coupled to cavity modes that can modify the symmetry of the ground-state wavefunction, and the polaritonic potential energy surfaces of the magnesium hydride ion coupled to a lossy photonic mode.

II. THEORY

We start with the Pauli-Fierz Hamiltonian in the dipole approximation in the length gauge, written in atomic units, following References 24, 27, and 31:

$$\hat{H} = \hat{H}_e + \hat{H}_p + \hat{H}_{dse} + \hat{H}_{ep}, \tag{1}$$

where

$$\hat{H}_e = \sum_i^{N_e} \hat{T}_e(x_i) + \sum_i^{N_e}\sum_A^{N_N} \hat{V}_{eN}(x_i;X_A) + \sum_i^{N_e}\sum_j^{N_e} \hat{V}_{ee}(x_i,x_j) + V_{NN}, \tag{2}$$

with $\hat{T}_e(x_i)$ denoting the electronic kinetic energy operator for electron i, $\hat{V}_{eN}(x_i;X_A)$ the (attractive) coulomb operator for electron i and nucleus A, $\hat{V}_{ee}(x_i,x_j)$ the (repulsive) coulomb operator for electrons i and j, and V_{NN} is the total (repulsive) coulomb potential between all of the nuclei. Within the Born-Oppenheimer approximation, V_{NN} is a constant, the nuclear kinetic energy is neglected, and the electron-nuclear attraction depends parametrically on the fixed nuclear coordinates. The photonic contribution is captured by the complex energy

$$\hat{H}_p = \tilde{\omega}\hat{b}^\dagger\hat{b}, \tag{3}$$

and the photon-molecule intereaction contains a bilinear coupling term,

$$\hat{H}_{ep} = -\sqrt{\frac{\tilde{\omega}}{2}}\left(\lambda\cdot(\hat{\mu}-\langle\mu\rangle)\right)\left(\hat{b}^{\dagger}+\hat{b}\right), \tag{4}$$

and a quadratic dipole self energy term,

$$\hat{H}_{dse} = \frac{1}{2}\left(\lambda\cdot(\hat{\mu}-\langle\mu\rangle)\right)^2. \tag{5}$$

In the above, $\hat{b}^{\dagger}$ and $\hat{b}$ are the bosonic raising/lowering operators for the photonic degrees of freedom, and $\tilde{\omega} = \omega - i\frac{\gamma}{2}$ is a complex frequency of the photon with the real part ω being related to the energy of the photon, and the imaginary part γ being related to the dissipation rate of the photonic degree of freedom[18,25,40]. The term $\langle\mu\rangle$ represents the ground state molecular dipole expectation value which has cartesian components $\xi \in \{x,y,z\}$. A given ξ-component of the dipole operator has the form $\hat{\mu}^{\xi} = \sum_i^{N_e}\hat{\mu}^{\xi}(x_i) + \mu_{nuc}^{\xi}$ where $\hat{\mu}^{\xi}(x_i)$ is an operator that depends on electronic coordinates and within the Born-Oppenheimer approximation, we treat the cartesian components of the nuclear dipole moment μ_{nuc}^{ξ} as functions of the nuclear coordinates rather than a quantum mechanical operator. Note that the shift of the Hamiltonian by $\langle\mu\rangle$ results from the transformation to the coherent state basis[24]. As we will see in the following section, solving the CQED-RHF equations will entail iterative updates to $\langle\mu\rangle$ with the CQED-RHF orbitals, and this expectation value can be initiated using the result from a canonical RHF calculation.

A. CQED-RHF

As our first step in approximating the energy eigenstates of Eq. 1, we follow Ref. 24 and 27 and introduce a product wavefunction between an electronic Slater determinant (which in practice may be initialized using a canonical RHF wavefunction) and a zero-photon number state,

$$|R\rangle = |\Phi_0\rangle|0\rangle. \tag{6}$$

To develop CQED-RHF theory, we examine the expectation value of Eq.1 with respect to Eq. 6,

$$\begin{aligned}&\langle R|\hat{H}_{ep}|R\rangle + \langle 0|\hat{H}_p|0\rangle + \langle\Phi_0|\hat{H}_e + \hat{H}_{dse}|\Phi_0\rangle \\ &= \langle\Phi_0|\hat{H}_e|\Phi_0\rangle + \langle\Phi_0|\hat{H}_{dse}|\Phi_0\rangle,\end{aligned} \tag{7}$$

where we see that the terms involving $\hat{H}_p$ and $\hat{H}_{ep}$ vanish, and the expectation value of $\hat{H}_e$ is analogous to the ordinary RHF energy. To evaluate the expectation value of $\hat{H}_{dse}$, we can first expand $\hat{H}_{dse}$ in terms of the dipole operator (with electronic and nuclear contributions) and dipole expectation values as follows:

$$\begin{aligned}\hat{H}_{dse} = &\sum_{\xi,\xi'}\sum_{i,j>i}\lambda^{\xi}\lambda^{\xi'}\hat{\mu}^{\xi}(x_i)\hat{\mu}^{\xi'}(x_j) \\ &-\frac{1}{2}\sum_{\xi,\xi'}\sum_i\lambda^{\xi}\lambda^{\xi'}\hat{Q}^{\xi\xi'}(x_i) \\ &+(\lambda\cdot\mu_{nuc}-\lambda\cdot\langle\mu\rangle)\sum_{\xi}\sum_i\lambda^{\xi}\hat{\mu}^{\xi}(x_i) \\ &+\frac{1}{2}(\lambda\cdot\mu_{nuc})^2-(\lambda\cdot\langle\mu\rangle)(\lambda\cdot\mu_{nuc})+\frac{1}{2}(\lambda\cdot\langle\mu\rangle)^2\end{aligned} \tag{8}$$

In the above expansion of $\hat{H}_{dse}$ we have specifically indicated that the product of electronic dipole operators contains 2-electron contributions when $i \neq j$, and 1-electron quadrupole contributions when $i = j$. The quadrupole contributions arise from the fact that $\hat{\mu}^{\xi}(x_i)\hat{\mu}^{\xi'}(x_i) = -\hat{Q}^{\xi\xi'}(x_i)$. Furthermore, a one-electron term arises that contains the electronic dipole operator scaled by $\lambda\cdot\mu_{nuc}-\lambda\cdot\langle\mu\rangle$, where again $\langle\mu\rangle$ will be iteratively updated during the CQED-RHF procedure.

To solve the CQED-RHF equations, the additional one-electron terms above will be added to the typical core Hamiltonian elements $h_{\mu\nu}$ that arises in canonical Hartree-Fock theory, and the additional two-electron terms above will be included in the density-matrix dependent terms in the Fock operator:

$$F_{\mu\nu} = H_{\mu\nu} + G_{\mu\nu} \tag{9}$$

where

$$\begin{aligned}H_{\mu\nu} = h_{\mu\nu} &-\frac{1}{2}\sum_{\xi,\xi'}\lambda^{\xi}\lambda^{\xi'}Q_{\mu\nu}^{\xi\xi'} \\ &+(\lambda\cdot\mu_{nuc}-\lambda\cdot\langle\mu\rangle)\sum_{\xi}\lambda^{\xi}\mu_{\mu\nu}^{\xi}\end{aligned} \tag{10}$$

and

$$\begin{aligned}G_{\mu\nu} = &(2(\mu\,\nu\,|\,\lambda\,\sigma) - (\mu\,\lambda\,|\,\nu\,\sigma))D_{\lambda\sigma} \\ &+\left(\sum_{\xi\xi'}\lambda^{\xi}\lambda^{\xi'}\left(2\mu_{\mu\nu}^{\xi}\mu_{\lambda\sigma}^{\xi'} - \mu_{\mu\lambda}^{\xi}\mu_{\nu\sigma}^{\xi'}\right)\right)D_{\lambda\sigma},\end{aligned} \tag{11}$$

leading to the total QED-RHF energy being

$$E_{CQED-RHF} = (F_{\mu\nu}+H_{\mu\nu})D_{\mu\nu} + V_{NN} + d_c \tag{12}$$

where

$$d_c = \frac{1}{2}(\lambda\cdot\mu_{nuc})^2 - (\lambda\cdot\langle\mu\rangle)(\lambda\cdot\mu_{nuc}) + \frac{1}{2}(\lambda\cdot\langle\mu\rangle)^2. \tag{13}$$

For clarity, we briefly outline the CQED-RHF algorithm below:

1. Compute kinetic, nuclear attraction, electron repulsion, dipole, and quadrupole integrals in AO basis
2. Perform canonical RHF calculation
3. Initialize **D** and $\langle\mu\rangle$ from canonical RHF wavefunction

4. Augment core Hamiltonian with the dipole and quadrupole terms in Eq. 10
5. Augment the Fock matrix by contracting products of dipole integrals over current density matrix in Eq. 11
6. Compute SCF energy through Eq. 12
7. Diagonalize Fock matrix and update density matrix
8. Check for convergence; if not converged, return to step 5.

B. Non-Hermitian CQED-CIS in the CQED-RHF basis

A mean-field description of the excited states of the molecular system strongly interacting with photonic degrees of freedom, and a correction to the ground-state that contains coupling between the CQED-RHF reference and simultaneous electronic and photonic excitations, may be obtained through a configuration interaction singles (CIS) ansatz. Here we formulated a non-Hermitian version of such an ansatz, NH-CQED-CIS, that incorporates the dissipative features of the photonic degrees of freedom. In our presentation, we formulate NH-CQED-CIS in the coherent state basis using the orbitals that result from the CQED-RHF approach outlined above.

The polaritonic energy eigenfunctions for state I in the NH-CQED-CIS ansatz can be written as a linear combination of the CQED-RHF ground-state and products of all possible single excitations out of the CQED-RHF reference. The CQED-RHF reference involves the product of an electronic Slater determinant with the photon vacuum state, so single excitations can occur as electronic excitations from an occupied orbital ϕ_i to a virtual orbital ϕ_a, the raising of the photon number state from $|0\rangle \rightarrow |1\rangle$, or both. We therefore write the NH-QED-CIS wavefunction for state I as

$$\Psi_I = c_0^0|\Phi_0\rangle|0\rangle + c_0^1|\Phi_0\rangle|1\rangle + \sum_{i,a} c_{ia}^0|\Phi_i^a\rangle|0\rangle + \sum_{i,a} c_{ia}^1|\Phi_i^a\rangle|1\rangle. \tag{14}$$

where the coefficients c denote the contribution of a given term to the wavefunction and we have denoted the electronic excitations in the subscript and the photonic excitations in the superscript of these coefficients. These coefficients, and the corresponding energy eigenvalues for a given NH-CQED-CIS state I, may be obtained by diagonalizing the Hamiltonian matrix built in the basis shown in Eq. 14. We spin adapt this basis such that $|\Phi_i^a\rangle = \frac{1}{\sqrt{2}}\left(|\Phi_{i\alpha}^{a\alpha}\rangle + |\Phi_{i\beta}^{a\beta}\rangle\right)$, where α and β label the spin orbitals as being occupied by spin-up and spin-down electrons, respectively. There are three classes of matrix elements that contribute to the Hamiltonian matrix, and we we write each class of matrix elements after shifting the total Hamiltonian in Eq. 1 by $E_{CQED-RHF}$. The matrix elements involving the CQED-RHF electronic Slater determinant $|\Phi_0\rangle$ and photonic states $|s\rangle$ and $|t\rangle$, where $s,t \in \{0,1\}$ involve only the (complex) photonic energy,

$$\langle s|\langle\Phi_0|\hat{H} - E_{CQED-RHF}|\Phi_0\rangle|t\rangle = \tilde{\omega}\, t\, \delta_{st}. \tag{15}$$

Matrix elements coupling $|\Phi_0\rangle|s\rangle$ to $|\Phi_i^a\rangle|t\rangle$ involve only the $\hat{H}_{ep}$ contributions:

$$\begin{aligned}&\langle s|\langle\Phi_0|\hat{H} - E_{CQED-RHF}|\Phi_i^a\rangle|t\rangle = \\ &-\sqrt{\tilde{\omega}}\sqrt{t+1}\,\delta_{s,t+1}\sum_{\xi}\lambda^{\xi}\mu_{ia}^{\xi} \\ &--\sqrt{\tilde{\omega}}\sqrt{t}\,\delta_{s,t-1}\sum_{\xi}\lambda^{\xi}\mu_{ia}^{\xi}.\end{aligned} \tag{16}$$

Matrix elements coupling different singly excited electronic and/or photonic states involve all terms of the Hamiltonian, including the canonical CIS terms:

$$\begin{aligned}&\langle s\langle\Phi_i^a|\hat{H} - E_{CQED-RHF}|\Phi_j^b\rangle|t\rangle \\ &= (\varepsilon_a - \varepsilon_i + d_c + \tilde{\omega}\, t)\,\delta_{ij}\delta_{ab}\delta_{st} \\ &+ \delta_{st}\,(2(ia|jb) - (ij|ab)) \\ &+ 2\delta_{st}\sum_{\xi,\xi'}\lambda^{\xi}\lambda^{\xi'}\mu_{ia}^{\xi}\mu_{jb}^{\xi} \\ &- \delta_{st}\sum_{\xi,\xi'}\lambda^{\xi}\lambda^{\xi'}\mu_{ij}^{\xi}\mu_{ab}^{\xi} \\ &+ \sqrt{t+1}\,\delta_{s,t+1}\delta_{ij}\delta_{ab}\sqrt{\frac{\tilde{\omega}}{2}}\lambda\cdot\langle\mu\rangle \\ &+ \sqrt{t}\,\delta_{s,t-1}\delta_{ij}\delta_{ab}\sqrt{\frac{\tilde{\omega}}{2}}\lambda\cdot\langle\mu\rangle \\ &- \sqrt{t+1}\,\delta_{s,t+1}\delta_{ij}\delta_{ab}\sqrt{\frac{\tilde{\omega}}{2}}\sum_{\xi}\sum_{k}\lambda^{\xi}\mu_{kk}^{\xi} \\ &- \sqrt{t}\,\delta_{s,t-1}\delta_{ij}\delta_{ab}\sqrt{\frac{\tilde{\omega}}{2}}\sum_{\xi}\sum_{k}\lambda^{\xi}\mu_{kk}^{\xi} \\ &- \sqrt{t+1}\,\delta_{s,t+1}\delta_{ij}\sqrt{\frac{\tilde{\omega}}{2}}\sum_{\xi}\lambda^{\xi}\mu_{ab}^{\xi} \\ &- \sqrt{t}\,\delta_{s,t-1}\delta_{ij}\sqrt{\frac{\tilde{\omega}}{2}}\sum_{\xi}\lambda^{\xi}\mu_{ab}^{\xi} \\ &+ \sqrt{t+1}\,\delta_{s,t+1}\delta_{ab}\sqrt{\frac{\tilde{\omega}}{2}}\sum_{\xi}\lambda^{\xi}\mu_{ij}^{\xi} \\ &+ \sqrt{t}\,\delta_{s,t-1}\delta_{ab}\sqrt{\frac{\tilde{\omega}}{2}}\sum_{\xi}\lambda^{\xi}\mu_{ij}^{\xi}.\end{aligned} \tag{17}$$

Because this NH-CQED-CIS Hamiltonian is non-Hermitian, the left and right eigenvectors, which we will denote Ψ_I^L and Ψ_I^R for the left and right eigenvectors for the NH-CQED-CIS state I respectively, are not simply complex conjugates of each other. However, the left and right eigenvectors can be chosen to be biorthogonal, where biorthogonality implies[42]

$$\langle\Psi_I^L|\Psi_J^R\rangle = \delta_{IJ}. \tag{18}$$

Using a biorthogonal basis enables one to compute expectation values for a given state I (e.g. the energy or dipole moment) or transition values between states I and J (e.g. the transition dipole moment) using the left and right eigenvectors as

the bra and ket states[42]:

$$\langle O_I \rangle = \langle \Psi_I^L | \hat{O} | \Psi_I^R \rangle \tag{19}$$

and

$$\langle O_{IJ} \rangle = \langle \Psi_I^L | \hat{O} | \Psi_J^R \rangle. \tag{20}$$

In our reference implementation, we enforce biorthogonality using a scheme based on LU decomposition.

III. REFERENCE IMPLEMENTATIONS

We provide reference implementations using Psi4Numpy[41], which provides a simple NumPy interface to the Psi4[43] quantum chemistry engine. The code for these reference implementations can be freely accessed in the hilbert package[44,45]. Furthermore, to provide a no-installation option for interested users to experiment with these implementations, we utilize the ChemCompute project[46] to host the illustrative calculations discussed in the Results section below. Interested users can navigate to https://chemcompute.org/register to register for a free ChemCompute account. Following registration, interested users can run calculations described in Table I in the results section using the link in Ref. 47, the calculations described in Figure 1 using the link Ref. 48, the results described in Table II and Figure 2 using the link in Ref. 49, and the results illustrated in Figure 3 using the link within Ref. 50.

IV. RESULTS

We apply the CQED-RHF and NH-CQED-CIS approaches to a few simple polaritonic chemical systems. First we examine the ground-state of formaldehyde strongly coupled to a single photon mode, which has been explored in by several groups that have been developing density functional theory-based *ab initio*-QED methods[9,35]. We optimize the geometry of lone formaldehyde at the RHF/cc-pVDZ level and perform all calculations at that geometry (see Ref. 47). At this level, the RHF ground-state has a dipole moment oriented purely along the $z-$axis with $\langle \mu \rangle_z = -1.009$ atomic units. The CQED-RHF equations are solved for a fixed magnitude of the coupling vector $|\lambda| = 0.2$ atomic units with the following three polarizations: $\lambda_y = (0, |\lambda|, 0)$, $\lambda_z = (0, 0, |\lambda|)$, and $\lambda_{yz} = \left(0, \frac{|\lambda|}{\sqrt{2}}, \frac{|\lambda|}{\sqrt{2}}\right)$.

The ground-state energy, as predicted by the CQED-RHF method, departs from the RHF energy in all three cases, with the largest deviation coming from λ_z case (see Table I), which would be expected given the permanent dipole moment is oriented along the z-axis. However, the deviations seen by the λ_y and λ_{yz} cases point to subtle effects arising from the quadrupolar terms in the quadratic self energy and the 2-electron contribution to the quadratic self energy. To quantify these various contributions, we look at the changes in the various contributions to the CQED-RHF energy with and without coupling to the photon field. For example, we define the change in the canonical RHF 1-electron energy resulting from the photon field in the λ_{yz} case as

$$\Delta_{1E} = \sum_{\mu\nu} 2h_{\mu\nu} D_{\mu\nu}^{\lambda_{yz}} - 2h_{\mu\nu} D_{\mu\nu}, \tag{21}$$

where $D_{\mu\nu}^{\lambda_{yz}}$ are elements of the converged CQED-RHF density matrix in the λ_{yz} case and $D_{\mu\nu}$ are elements of the CQED-RHF density matrix in the absence of coupling to a photon (i.e., the canonical RHF density matrix). We tabulate the changes in these various CQED-RHF contributions for the λ_z, λ_y, and λ_{yz} cases in Table I.

Total	Canonical RHF		Cavity Contributions			
ΔE (a.u.)	% Δ_{1E}	% Δ_{2E}	% Δ_{1de}	% Δ_{1qe}	% Δ_{2de}	% Δ_{d_c}
λ_y						
0.135	-210	213	0	210	-113	0
λ_z						
0.161	-169	172	-23	440	-331	11
λ_{yz}						
0.148	-185	188	-12	333	-230	6

TABLE I. Change in total CQED-RHF energy (ΔE in atomic units) and % relative changes in different contributions to the total CQED-RHF energy for three different polarizations of a photonic mode with magnitude $|\lambda| = 0.2$ atomic units. The terms Δ_{1E} and Δ_{2E} denote changes in the RHF 1- and 2-electron energies, respectively, and the terms Δ_{1de}, Δ_{2de}, Δ_{1qe}, Δ_{d_c} denote changes in the CQED-RHF 1-electron dipole, 2-electron dipole, 1-electron quadrupole, and dipole constant terms respectively.

The 1-electron quadrupolar and 2-electron dipolar terms that arise from $\hat{H}_{dse}$ typically comprise the largest changes to the CQED-RHF energy from the three polarizations considered in Table I. However, the changes in the canonical RHF 1- and 2-electron terms (denoted Δ_{1E} and Δ_{2E}) suggest changes to the ground-state electron density via the CQED-RHF orbitals arise from coupling to the cavity modes. Although these changes largely cancel each other in the total energy (i.e. $\Delta_{1E} \approx -\Delta_{2E}$ in all three cases), it is nevertheless interesting to view the impact of cavity coupling on the CQED-RHF orbitals. The RHF orbitals for the HOMO ($2B_2$) and LUMO+1 ($6A_1$) of formaldehyde uncoupled to a photon are compared to their corresponding CQED-RHF orbitals for the λ_{yz} case ($7A^{'}$ and $8A^{'}$) where the orbitals are strikingly distorted (see Figure 1). The reshaping of the CQED-RHF orbitals in the λ_{yz} case results in a loss of symmetry from C_{2v} to C_s and impacts both ground-state energy and properties. As seen in Table I, there is no 1-electron dipole contribution to the energy shift in the λ_y case since the ground state dipole moment is oriented purely along the z-axis. However, in the λ_{yz} case, the distortion of the ground-state orbitals results in a reorientation of the dipole moment to point along the yz axis with value $\langle \mu \rangle = (0, -0.074, -1.16)$ atomic units. We see that this reorientation of the ground-state dipole moment is accompanied by changes in the ground-state energy specifically attributable to the 1-electron dipolar terms CQED-RHF Fock operator (see Table I).

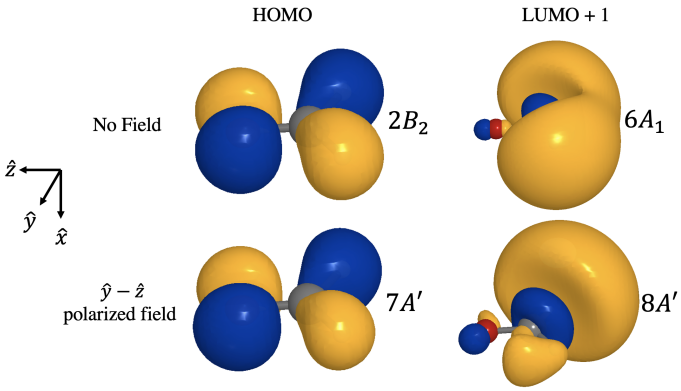

FIG. 1. Comparison of the HOMO and LUMO+1 orbitals of formaldehyde uncoupled to an photon mode (top) and strongly coupled to a photon mode polarized along the $y-z$ axis (bottom), where strong coupling results in a change in symmetry from C_{2v} to C_s.

Turning to the NH-CQED-CIS Hamiltonian, it can be seen that unlike the canonical CIS method, the NH-CQED-CIS method couples single excitations of the electronic and photonic terms to the CQED-RHF reference state. Specifically, it can be seen in Eq. (16) that the CQED-RHF wavefunction can couple to states which involve singly-excited electronic configurations and singly-occupied photon states. This coupling can lower the energy of the lowest energy eigenstate of the NH-CQED-CIS Hamiltonian relative to the ground-state determined by the CQED-RHF method (see Table II). The cavity-induced modification to the symmetry of the CQED-RHF wavefunction has important consequences for which singly-excited configurations can contribute to the ground state. We examine the impacts of this cavity effect again with formaldehyde coupled to a lossless photon with $\tilde{\omega}$ = 0.382 atomic units (10.4 eV), which is approximately resonant with the first two dipole allowed transitions at the CIS/cc-pVDZ level of theory (see Ref. 49). We consider the same coupling magnitudes as before, this time focusing only on the λ_z and λ_{yz} cases. The polarization vector in the λ_z case belongs to the A_1 irrep of the C_{2v} point group, while the polarization vector in the λ_{yz} case belongs to the $A^{'}$ irrep of the C_s point group. In Figure 2, we present the dominant singly-excited contributions to the NH-CQED-CIS ground-state in the λ_z and λ_{yz} cases. We indeed see slightly more permissive mixing of singly-excited configurations into the NH-CQED-CIS ground-state in the λ_{yz} case due to the lower symmetry of the wavefunction. We report the changes in the ground-state energy as predicted by the NH-CQED-CIS method relative to the canonical RHF method and the CQED-RHF method in Table II.

As a second illustrative example of the NH-CQED-CIS method, we consider the upper-polariton ($|UP\rangle$) and lower-polariton ($|LP\rangle$) states that emerge from coupling MgH^+ to a photon resonant with the ground to first singlet excited state ($|X\rangle \rightarrow |A\rangle$) transition[23]. We consider the photon to be polarized along the z axis, in alignment with the relevant transition dipole moment, with λ_z = 0.0125 atomic units. This time, we allow the photon to have a complex energy where

	Relative to RHF	Relative to CQED-RHF
Polarization	ΔE (a.u.)	ΔE (a.u.)
λ_z	0.123	-0.038
λ_{yz}	0.116	-0.032

TABLE II. Changes in the ground-state energy predicted by the NH-CQED-CIS method relative to the canonical RHF energy as well as the CQED-RHF energy in atomic units. Calculations were performed with a fixed magnitude of $|\lambda| = 0.2$ atomic units for the λ_z and λ_{yz} polarizations. NH-CQED-CIS method calculations were performed to reflect formaldehyde coupling to a photon with $\tilde{\omega} = 0.382$ atomic units.

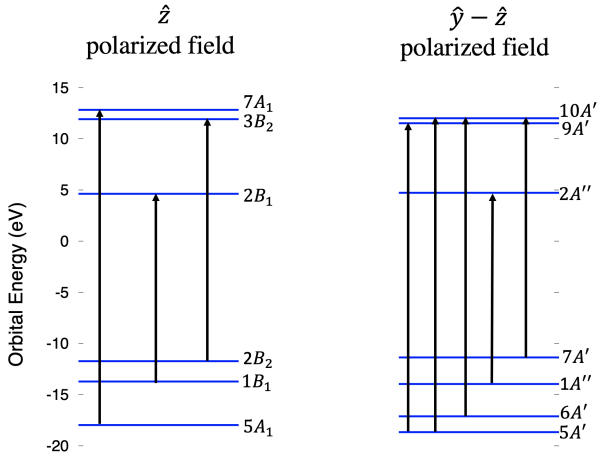

FIG. 2. Dominant single excitations from the CQED-RHF reference that contribute to the NH-CQED-CIS ground-state wavefunction when formaldehyde is coupled to a photon with $\tilde{\omega} = 0.382$ atomic units (10.4 eV) polarized along the z axis with $\lambda_z = 0.2$ atomic units (left) and $y-z$ axes (right) with $\lambda_y = \lambda_z = \sqrt{2}/2$ atomic units (right).

the imaginary part accounting for photonic dissipation, which can also be related to the energy uncertainty of the photonic mode[25]. We consider the real part of the photon energy to be 4.75 eV, and the imaginary part to be either 0 eV or 0.22 eV. The two lowest-lying excited states of the NH-CQED-CIS with both photon frequency values are plotted as a function of bondlength for values between 1.3 and 2.7 Angstroms with increments of 0.1 Angstroms (see Ref. 50) in Figure 3. In addition to computing these polariton surfaces at the NH-CQED-CIS/cc-pVDZ level, we compute these polaritonic surfaces at the same values of the MgH+ bondlength R using a model 3-level Hamiltonian:

$$\mathbf{H} = \begin{pmatrix} E_X + \frac{(\lambda\cdot\langle\mu_X\rangle)^2}{2} & 0 & 0 \\ 0 & E_X + \tilde{\omega} + \frac{(\lambda\cdot\langle\mu_X\rangle)^2}{2} & \sqrt{\frac{\tilde{\omega}}{2}}\lambda\cdot\mu_{XA} \\ 0 & \sqrt{\frac{\tilde{\omega}}{2}}\lambda\cdot\mu_{XA} & E_A + \frac{(\lambda\cdot\langle\mu_A\rangle)^2}{2}. \end{pmatrix} \tag{22}$$

In Eq. (22), E_X ($\langle\mu_X\rangle$) and E_A ($\langle\mu_A\rangle$) denote the ground-state and first singlet excited-state energies (dipole moments), respectively, and μ_{XA} denotes the transition dipole moment between state X and A. The ground-state energies and dipole moments for each value of R are calculated at the RHF/cc-

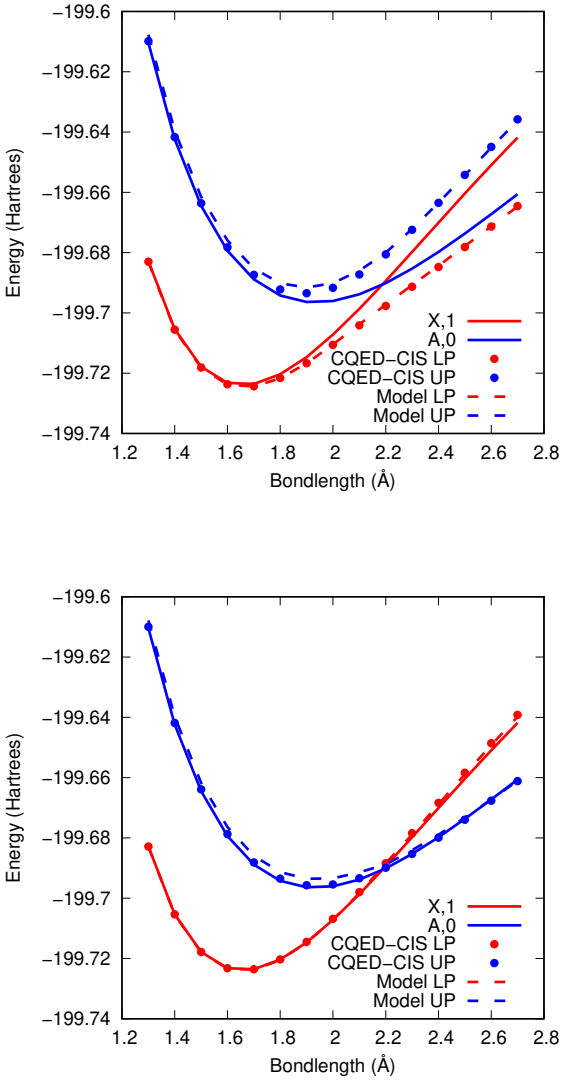

FIG. 3. Polaritonic surface of MgH+ coupled to a photon with (top) $\hbar\tilde{\omega} = 4.75$ eV and (bottom) $\hbar\tilde{\omega} = 4.75 - 0.22$ eV with $\lambda_z = 0.0125$ atomic units. We see evidence of strong coupling via splitting of the surfaces where the $|X,1\rangle$ and $|A,0\rangle$ states are resonant, when the photon energy is pure real, and we see the splitting vanish when the imaginary part of the photon energy is large compared to the interaction energy.

pVDZ level and the excited-state energies, dipole moments, and transition dipole moments are calculated at the CIS/cc-pVDZ level (see Ref. 50). The polaritonic surfaces obtained from diagonalizing Eq. (22) are referred to as the 'Model LP' and 'Model UP' surfaces in Figure 3. We see with a pure real photon energy, the $|LP\rangle$ and $|UP\rangle$ surfaces experience a strong splitting in the region where the $|X,1\rangle$ state (the ground-state plus a photon) crosses the $|A,0\rangle$ state (the first excited-state without a photon). It should be noted that the NH-CQED-CIS curves are typically slightly stabilized compared to the Model LP and UP curves. We have already seen that the CQED-RHF method can provide orbital relaxation in the presence of cavity coupling that would not be available to the Model LP and UP solutions, and the NH-CQED-CIS wavefunction also includes additional variational flexibility through the excitations coupled through the $\hat{H}_{dse}$ and $\hat{H}_{ep}$ terms. For a strongly dissipative photon, we see that both the model and CQED-CIS curves closely approximate the CIS curves for the lone molecules, which signals that this system is not in the strong-coupling regime. The loss of strong coupling in this case arises because the dissipative energy scale of the photon is significant compared to the interaction energy scale between the photon and the molecular transition[25]. This echos a fundamental condition for strong coupling that the interaction strength V must be large compared to the dissipation energy scale $\hbar\gamma$, specifically $V > \hbar\frac{\gamma}{4}$. If this condition is not satisfied, then the energy splitting between the interacting states vanishes. The imaginary part of the frequency giving rise to the curves shown in the bottom panel of Figure 3 was specifically chosen so that $V < \hbar\frac{\gamma}{4}$, leading to the vanishing of the splitting that is observed in the top panel of Figure 3.

V. CONCLUSIONS

We combined *ab initio* molecular electronic Hamiltonians with a cavity quantum electrodynamics model for dissipative photonic modes and applied mean-field theories to the ground- and excited-states of resulting polaritonic systems. In particular, we developed a restricted Hartree-Fock theory for the mean-field ground-state and a non-Hermitian configuration interaction singles theory for mean-field ground- and excited-states of the molecular system strongly interacting with a photonic mode, and applied these methods to elucidating the phenomenology of paradigmatic polaritonic systems. These methods were applied to the analysis of several paradigmatic systems, including the ground-state polaritonic structure of formaldehyde coupled to cavity modes that were shown to modify the symmetry of the ground-state wavefunction, and the polaritonic potential energy surfaces of the magnesium hydride ion coupled to a lossy photonic mode. A reference implementation of both methods was realized using the Psi4Numpy framework which can be accessed using links provided within the text.

ACKNOWLEDGMENTS

JM and JJF Acknowledges support from the Research Corporporation for Scientific Advancement Cottrell Scholar Award and the NSF CAREER Award CHE-2043215. Computational resources were provided in part by the MERCURY consortium (http://mercuryconsortium.org/) under NSF grants CHE-1229354, CHE-1662030, and CHE-2018427. We gratefully acknowledge A. E. DePrince III for numerous helpful discussions and access to benchmark results for the CQED-RHF method.

VI. DATA AVAILABILITY STATEMENT

The data that support the findings of this study are available upon request, and the source code and scripts used to generate the reported data are publicly available on GitHub at https://github.com/FoleyLab/psi4polaritonic and may be run using the links provided in Refs. 47–50.

[1] J. A. Hutchison, T. Schwartz, C. Genet, E. Devaux, and T. W. Ebbesen, "Modifying chemical landscapes by coupling to vacuum fields," Angew. Chem. Int. Ed. Engl. **13**, 1592–1596 (2012).

[2] J. Galego, F. J. Garcia-Vidal, and J. Feist, "Cavity-induced modifications of molecular structure in the strong-coupling regime," Phys. Rev. X **5**, 041022 (2015).

[3] T. W. Ebbesen, "Hybrid light-matter states in a molecular and material science perspective," Acc. Chem. Res. **49**, 2403–2412 (2016).

[4] F. Herrera and F. C. Spano, "Cavity-controlled chemistry in molecular ensembles," Phys. Rev. Lett. **116**, 238301 (2016).

[5] N. M. Hoffmann, H. Appel, A. Rubio, and N. T. Maitra, "Light-matter interactions via the exact factorization approach," Eur. Phys. J. B **91**, 180 (2018).

[6] J. Feist, J. Galego, and F. J. Garcia-Vidal, "Polaritonic chemistry with organic molecules," ACS Photonics **5**, 205–216 (2018).

[7] L. A. Martinez-Martinez, R. F. Ribeiro, J. Campos-Gonzalez-Angulo, and J. Yuen-Zhou, "Can ultrastrong coupling change ground-state chemical reactions?" ACS Photonics **5**, 167–176 (2018).

[8] B. Munkhbat, M. Wersäll, D. G. Baranov, T. J. Antosiewicz, and T. Shegai, "Suppression of photo-oxidation of organic chromophores by strong coupling to plasmonic nanoantennas," Sci. Adv. **4**, eaas9552 (2018).

[9] J. Flick and P. Narang, "Cavity-correlated electron-nuclear dynamics from first principles," Phys. Rev. Lett. **121**, 113002 (2018).

[10] J. Fregoni, G. Granucci, E. Coccia, M. Persico, and S. Corni, "Manipulating azobenzene photoisomerization through strong light–molecule coupling," Nat. Commun. **9**, 4688 (2018).

[11] L. A. Martínez-Martínez, M. Du, R. F. Ribeiro, S. Kéna-Cohen, and J. Yuen-Zhou, "Polariton-assisted singlet fission in acene aggregates," J. Phys. Chem. Lett. **9**, 19511957 (2018).

[12] L. A. Martínez-Martínez, E. Eizner, S. Kéna-Cohen, and J. Yuen-Zhou, "Triplet harvesting in the polaritonic regime: A variational polaron approach," J. Chem. Phys. **151**, 054106 (2019).

[13] O. D. Stefano, A. Settineri, V. Macri, L. Garziano, R. Stassi, S. Savasta, and F. Nori, "Resolution of gauge ambiguities in ultrastrong-coupling cavity quantum electrodynamics," Nat. Phys. **15**, 803–808 (2019).

[14] M. Du, R. F. Ribeiro, and J. Yuen-Zhou, "Remote control of chemistry in optical devices," Chem. Cell. Press **5**, 1167–1181 (2019).

[15] A. Mandal and P. Huo, "Investigating new reactivities enabled by polariton photochemistry," J. Phys. Chem. Lett. **10**, 5519–5529 (2019).

[16] A. Mandal, T. D. Krauss, and P. Huo, "Polariton-mediated electron transfer via cavity quantum electrodynamics," J. Phys. Chem. B (2020).

[17] M. A. D. Taylor, A. Mandal, W. Zhou, and P. Huo, "Resolution of gauge ambiguities in molecular cavity quantum electrodynamics," Phys. Rev. Lett. (2020).

[18] S. Felicetti, J. Fregoni, T. Schnappinger, S. Reiter, R. de Vivie-Riedle, and J. Feist, "Photoprotecting uracil by coupling with lossy nanocavities," J. Phys. Chem. Lett. **11**, 8810 (2020).

[19] J. Fregoni, S. Corni, M. Persico, and G. Granucci, "Photochemistry in the strong coupling regime: A trajectory surface hopping scheme," J. Comput. Chem. **41**, 2033–2044 (2020).

[20] J. Fregoni, G. Granucci, M. Persico, and S. Corni, "Strong coupling with light enhances the photoisomerization quantum yield of azobenzene," Chem **6**, 250–265 (2020).

[21] I. S. Ulusoy and O. Vendrell, "Dynamics and spectroscopy of molecular ensembles in a lossy microcavity," J. Chem. Phys. **153**, 044108 (2020).

[22] N. M. Hoffman, L. Lacombe, A. Rubio, and N. T. Maitra, "Effect of many modes on self-polaritzation and photochemical suppression in cavities," J. Chem. Phys. **153**, 104103 (2020).

[23] E. Davidsson and M. Kowalewski, "Simulating photodissociation reactions in bad cavities with the lindblad equation," J. Chem. Phys. **153**, 234304 (2020).

[24] T. S. Haugland, E. Ronca, E. F. Kjønstad, A. Rubio, and H. Koch, "Coupled cluster theory for molecular polaritons: Changing ground and excited states," Phys. Rev. X **10**, 041043 (2020).

[25] P. Antoniou, F. Suchanek, J. F. Varner, and J. J. F. IV, "Role of cavity losses on nonadiabatic couplings and dynamics in polaritonic chemistry," J. Phys. Chem. Lett. **11**, 9063–9069 (2020).

[26] M. H. Farag, A. Mandal, and P. Huo, "Polariton induced conical intersection and berry phase," Phys. Chem. Chem. Phys. **23**, 16868 (2021).

[27] A. E. D. III, "Cavity-modulated ionization potentials and electron affinities from quantum electrodynamics coupled-cluster theory," J. Chem. Phys. **154**, 094112 (2021).

[28] M. Du, J. C. G. Angulo, and J. Yuen-Zhou, "Nonequilibrium effects of cavity leakage and vibrational dissipation in thermally-activated polariton chemistry," J. Chem. Phys. **154**, 084108 (2021).

[29] J. Torres-Sánchez and J. Feist, "Molecular photodissociation enabled by ultrafast plasmon decay," J. Chem. Phys. **154**, 014303 (2021).

[30] I. V. Tokatly, "Time-dependent density functional theory for many-electron systems interacting with cavity photons," Phys. Rev. Lett. **110**, 23301 (2013).

[31] M. Ruggenthaler, N. Tancogne-Dejean, J. Flick, H. Appel, and A. Rubio, "From a quantum-electrodynamical light–matter description to novel spectroscopies," Nat. Rev. Chem. **2**, 0118 (2018).

[32] J. Flick and P. Narang, "Ab initio polaritonic potential-energy surfaces for excited-state nanophotonics and polaritonic chemistry," J. Chem. Phys. **153**, 094116 (2020).

[33] U. Mordovina, C. Bungey, K. Appel, P. J. Knowles, A. Rubio, and F. R. Manby, "Polaritonic coupled-cluster theory," Phys. Rev. Research **2**, 023262 (2020).

[34] F. Buchholz, I. Theophilou, S. E. B. Nielsen, M. Ruggenthaler, and A. Rubio, "Reduced density-matrix approach to strong matter-photon interaction," ACS Photonics **6**, 2694–2711 (2019).

[35] J. Yang, Q. Ou, Z. Pei, H. Wang, B. Weng, Z. Shuai, K. Mullen, and Y. Shao, "Quantum-electrodynamical time-dependent density functional theory within gaussian atomic basis," J. Chem. Phys. **155**, 064107 (2021).

[36] M. Ruggenthaler, F. Mackenroth, and D. Bauer, "Timedependent kohn-sham approach to to quantum electrodynamics," Phys. Rev. A **84**, 042107 (2011).

[37] M. Ruggenthaler, J. Flick, C. Pellegrini, H. Appel, I. V. Tokatly, and A. Rubio, "Quantum-electrodynamical density-functional theory: Bridging quantum optics and electronic structure theory," Phys. Rev. A **90**, 012508 (2014).

[38] C. Pellegrini, J. Flick, I. V. Tokatly, H. Appel, and A. Rubio, "Optimized effective potential for quantum electrodynamical time-dependent density functional theory," Phys. Rev. Lett. **115**, 093001 (2015).

[39] R. Jestädt, M. Ruggenthaler, M. J. T. Oliveira, A. Rubio, and H. Appel, "Light-matter interactions within the ehrenfest–maxwell–pauli–kohn–sham framework: fundamentals, implementation, and nano-optical applications," Adv. Phys. **68**, 225–333 (2019).

[40] C. L. Cortes, M. Otten, and S. K. Gray, "Non-hermitian approach for quantum plasmonics," J. Chem. Phys. **152**, 084105 (2020).

[41] D. G. A. Smith, L. A. Burns, D. A. Sirianni, D. R. Nascimento, A. Kumar, A. M. James, J. B. Schriber, T. Zhang, B. Zhang, A. S. Abbott, E. J. Berquist, M. H. Lechner, L. A. Cunha, A. G. Heide, J. M. Waldrop, T. Y. Takeshita, A. Alenaizan, D. Neuhauser, R. A. King, A. C. Simmonett, J. M. Turney, H. F. Schaefer, F. A. Evangelista, A. E. D. III, T. D. Crawford, K. Patkowski, and C. D. Sherrill, "Psi4numpy: An interactive quantum chemistry programming environment for reference implementations and rapid development," J. Chem. Theor. Comput. **14**, 3504–3511 (2018).

[42] J. F. Stanton and R. J. Bartlett, "The equation of motion coupledcluster method. a systematic biorthogonal approach to molecular excitation energies, transition probabilities, and excited state properties," J. Chem. Phys. **98**, 7029 (1993).

[43] J. M. Turney, A. C. Simmonett, R. M. Parrish, E. G. Hohenstein, F. Evangelista, J. T. Fermann, B. J. Mintz, L. A. Burns, J. J. Wilke, M. L. Abrams, N. J. Russ, M. L. Leininger, C. L. Janssen, E. T. Seidl, W. D. Allen, H. F. Schaefer, R. A. King, E. F. Valeev, C. D. Sherrill, and T. D. Crawford, "Psi4: An open-source ab initio electronic structure program," WIREs Comput. Mol. Sci. **2**, 556 (2012).

[44] A. E. D. III, `https://github.com/edeprince3/hilbert` (2021), [Online; accessed 18-August-2021].

[45]J. McTague and J. J. F. IV, https://github.com/edeprince3/hilbert/tree/master/src/psi4numpy (2021), [Online; accessed 18-August-2021].
[46]M. J. Perri and S. H. Weber, "Web-based job submission interface for the gamess computational chemistry program," J. Chem. Educ. **91**, 2206–2208 (2014).
[47]J. McTague and J. J. F. IV, https://bit.ly/3aX03HK (2021), [Online; accessed 20-October-2021].
[48]J. McTague and J. J. F. IV, https://bit.ly/2ZdTsGH (2021), [Online; accessed 20-October-2021].
[49]J. McTague and J. J. F. IV, https://bit.ly/3B3U8v4 (2021), [Online; accessed 20-October-2021].
[50]J. McTague and J. J. F. IV, https://bit.ly/3lZ58ph (2021), [Online; accessed 20-October-2021].